Journal of Power Sources 622 (2024) 235375

Contents lists available at ScienceDirect

Journal of Power Sources

journal homepage: www.elsevier.com/locate/jpowsour

Inductive loops in impedance spectra of PEM water electrolyzers

Debora Brinker [a,*], Niklas Hensle [a,b], Jerónimo Horstmann de la Viña [b], Irene Franzetti [b], Lena V. Bühre [c], Umesh Anirudh Andaluri [b], Charlotte Menke [b], Tom Smolinka [b], André Weber [a]

[a] Institute for Applied Materials (IAM-ET), Karlsruhe Institute of Technology (KIT), Adenauerring 20b, 76131, Karlsruhe, Germany
[b] Fraunhofer Institute for Solar Energy Systems ISE, Heidenhofstrasse 2, 79110, Freiburg, Germany
[c] Leibniz University Hannover, Institute of Electric Power Systems, Appelstraße 9a, 30167, Hannover, Germany

HIGHLIGHTS

- Inductive effects at low frequencies affect the DC performance of the cell.
- Temperature and current density/voltage strongly affect the inductive behavior.
- They are only observable in the spectra of the anode.
- There is an overlap between mass transport and inductive processes.
- The membrane thickness has a strong influence on the inductive effects.

ARTICLE INFO

Keywords:
PEM electrolysis
EIS
Distribution of relaxation times
Inductive loops
Low frequency
Negative polarization resistance

ABSTRACT

Inductive loops at low frequencies in impedance spectra of proton exchange membrane (PEM) water electrolysis cells remain largely unexplored, yet they hold potential for performance enhancement due to their positive impact on the overall cell resistance.

This study investigates inductive loops at low frequencies by impedance spectroscopy and subsequent Distribution of Relaxation Times (DRT) analysis. The positive impact of the inductive loops is verified by voltage current scan measurements. Variations of operational and structural parameters, like membrane and catalyst layer properties and impregnated porous transport layers are performed to understand the origin of the inductive feature and its interplay with mass transport related processes.

Our findings reveal a significant impact of current density and voltage, temperature and membrane thickness on the inductive loop. Measurements via reference electrodes show a stronger correlation to the anode. Mass transport losses and the inductive loops are occurring in similar frequency ranges. Such overlapping of both effects with apparently positive and negative resistances can result in compensation in the spectra. The size of the inductive loops, which might even exceed the capacitive polarization resistance, and their dependence on the membrane thickness indicate that processes in the membrane are responsible for the observed behavior.

1. Introduction

Understanding electrochemical and transport processes within PEM water electrolysis cells is crucial for their development. Electrochemical Impedance Spectroscopy (EIS) and a subsequent impedance data analysis by the Distribution of Relaxation Times (DRT) is a well-established approach to detect, deconvolute and quantify the different polarization phenomena. However, in the context of PEM water electrolysis, EIS has predominantly focused on capacitive processes [1–6] neglecting the significant impact of pseudo inductive processes apparent as inductive loops in the low-frequency region of impedance spectra.

Most reported work in PEM water electrolysis uses impedance-based measurements to only determine the high frequency resistance (HFR) for a subsequent voltage losses break-down analysis using the Tafel approach, see for example [7–10]. Other works focus on the determination of charge transfer resistances using EIS coupled with equivalent circuit modeling (ECM) [6,11]. Analysis of the low-frequency impedance to understand capacitive polarization phenomena, related to mass

* Corresponding author.
E-mail address: debora.brinker@kit.edu (D. Brinker).

https://doi.org/10.1016/j.jpowsour.2024.235375
Received 24 June 2024; Received in revised form 30 August 2024; Accepted 1 September 2024
Available online 9 September 2024

transport is not as established for PEM water electrolysis as compared with PEM fuel cells. Different equivalent circuit models with a varying number of elements are reported [4,12,13]. Some works show low-frequency capacitive features without deeper focus on the impedance analysis, e.g. Refs. [14,15].

While literature for other electrochemical systems offers explanations for the origin of such low frequency inductive loops [16], such as the formation of intermediates like hydrogen peroxide [17], platinum oxide formation and its dissolution [18], and water diffusion processes [18,19] in PEM fuel cells. To the best of our knowledge only Ferriday a Middleton reported on the "pseudo-inductive demeanour" in PEM water electrolysis and referred it to diffusion and adsorption processes [20]. In our recent publication [21] we discussed existing literature on inductive loops for different electrochemical applications and demonstrate the existence of inductive loops in impedance spectra of PEM water electrolysis cells for various cell housing, porous transport layers (PTL), catalyst-coated membranes (CCM) and test bench combinations and validated the positive impact of its negative resistance on the cell performance.

The low frequency inductive loops are observed at frequencies <20 Hz. At these frequencies capacitive processes mostly related to diffusive and convective mass transport are observable. Various experimental investigations and electrochemical models are reported on mass transport processes in PEM water electrolysis [22–27]. Most of the published studies investigate diffusion processes without the use of EIS and do not explicitly consider the inductive behavior at low frequencies.

This current investigation delves deeper into understanding the origins of this inductive loop and how it can be used to enhance performance. We systematically explore various operational parameter variations and material interventions with the use of on adapted version of the DRT analysis. We discuss the superimposing of mass transport processes by inductive cell behavior which is in our opinion essential to discuss diffusion related polarization at current densities >1 A•cm^{-2}. Conclusively, we present and rate developed hypotheses on which physical processes can be related to the inductive loop based on PEM fuel cell and electrolysis knowledge.

2. Experimental

To investigate the inductive behavior in detail, we employ different experimental methods. We therefore test at different test facilities. We examine the inductive behavior via two different reference electrode setups and change different material parameters such as impregnated PTLs, anode catalyst layer properties and membrane thickness. A detailed introduction on testing facilities and cell setups is given in the following parts.

2.1. Test benches

In this study mostly two test benches at KIT and Fraunhofer ISE are used. The measurements via reference electrodes were conducted at two suitable test benches which are specifically made for their purpose at Fraunhofer ISE as well as at Leibniz University Hannover.

2.1.1. Greenlight Innovation test bench

At KIT a commercial *E20 Electrolyser Test Station* from *Greenlight Innovation* is employed. The test bench can operate at pressures of up to 5 barg (balanced and differential), water flow rates at the anode of up to 75 ml•min^{-1} and temperatures of up to 80 °C. The DI process water is not recirculated. After separation from the product gas, it is drained from the system. The temperature is controlled via the heated inlet water. The test bench in the present version is not equipped with an electrochemical workstation. Therefore, the test cell is connected externally to an electrochemical workstation by *Zahner Elektrik GmbH*, Germany. The employed workstation is a *Zahner Zennium X* connected to a *Zahner PP241*. With this configuration an operation of currents up to 40 A is possible.

2.1.2. Fraunhofer ISE test bench 1

The inhouse-built test bench used at Fraunhofer ISE is well-established and already presented in former publications [28,29]. The test bench was designed for an operation up to 50 bar, flow rates between 80 ml•min^{-1} and 2500 ml•min^{-1} and temperatures up to 80 °C. The test bench is equipped with an electrochemical workstation by *Zahner Elektrik GmbH*, Germany. For the use of small test cells, a *Zahner Zennium Pro* is connected to a *Zahner PP242* to measure operation points up to 40 A. The process water in the test bench is circulated and purified using inline ion exchangers. With this test bench it is possible to feed the water to the anode and the cathode separately. For a more detailed understanding we refer to the mentioned publications.

2.1.3. Fraunhofer ISE test bench 2 – reference electrode measurements

The test bench used for the reference electrode measurements at Fraunhofer ISE is in-house built. It is an ambient pressure test bench with the possibility to feed the anode and cathode with water separately from each other. To ensure high water quality, inline ion exchangers are used. The temperature can be controlled on the inlet or outlet temperature using inline sensors in the water and water-gas stream. Electrochemical characterization is carried out using a potentiostat system by *Zahner Elektrik GmbH*, Germany including Zahner Zennium Pro with the opportunity to measure five voltages in parallel, Zahner EL1000 and a third-party power supply.

2.1.4. Leibnitz University Hannover test bench – reference electrode measurements

The reference electrode measurements with the salt bridge approach are conducted at Leibnitz University of Hannover, see section Test cells with reference electrodes and discussion in Fig. 4 c) and d). The test bench used here is custom designed. The water can be applied to the anode using peristaltic pumps. Inline water filter ensures high water quality. For temperature control a heat recuperator and chiller is employed. The measurements are carried out with a SP150 Potentiostat and a 20 A booster from Bio-Logic SAS, France.

2.2. Test cell

For this study a 4 cm^2 test cell produced in-house by Fraunhofer ISE is used. The test cell housing consists of two identical titanium bodies with straight parallel flow fields consisting of ten milled flow channels each with a cross sectional area of 1 × 1 mm^2, the lands in between the channels have a width of 0.9 mm. On the titanium body a polymer frame is screwed which can be easily changed to use different PTL materials. Around the active area flat sealings produced by *Freudenberg FST GmbH*, Germany are used. The two parts with included PTLs and the CCM are stacked together and compressed using a compression cage with a centered screw. To monitor the clamping pressure applied, a force sensor by *Lorenz Messtechnik GmbH*, Germany is implemented. A bore in the center of the cell right underneath the flow field gives the possibility to measure the temperature very close to the CCM. The electrical connection is done by 4 mm holes in the cell body using banana plug connectors for the current and the voltage cables. A more detailed description of the test cell can be found elsewhere [28]. To ensure a

proper data reproducibility the clamping pressure distribution on the active area is determined using pressure paper by Fujifilm, Japan before each measurement series. Since we use titanium-based PTLs at anode and cathode, a minimum clamping pressure of 3 MPa for a proper internal contacting is employed.

For the reference electrode measurement two other test cells are used. One is built up by Fraunhofer ISE with 23 cm^2 active area, the other is a modification of the 4 cm^2 Fraunhofer ISE test cell to include a salt bridge reference electrode by Leibnitz University of Hannover, see section Test cells with reference electrodes.

2.3. Standard PTL and CCM

The CCM used in this study is commercially available with a Pt/C-based cathode catalyst layer and an IrOx-based anode catalyst layer. The membrane employed is a 125 μm Nafion® N115 membrane. For the PTLs platinum coated titanium fiber material with a thickness of 0.25 mm is used at anode and cathode. For the studies of reference electrode, anode catalyst and membrane thickness variation the materials differ, see respective sections.

2.4. Test cells with reference electrodes

To separate the anodic and cathodic polarization processes a test cell with implemented reference electrode can be a helpful approach [30–32]. In this study we employ two different types of reference electrodes to identify whether the inductive process occurs at anode, cathode or both electrodes. Therefore, one test cell developed by Fraunhofer ISE and another one by Leibniz University Hannover is used.

The test cell at Fraunhofer ISE presents an active area of 23 cm^2 next to a reference electrode of 1 cm^2 created by laser ablation. The concept was presented by Gerteisen [33] in a case study on fuel cells. The reference electrode employs a concept of a catalyst electrically isolated from the active catalyst layer without harming the membrane. The electrical isolation is enabled by segmented bipolar plates and PTLs. The laser ablation allows for a very good alignment of the electrode catalyst layers and, therefore, a homogenous distribution of the potentials [33,34]. The spectra are collected applying reference electrodes present on the anode and cathode. This approach should enable a separation of polarization phenomena at anode and cathode, respectively. It should be noted that contributions from a portion of the membrane and from the catalyst layer-membrane interface as well as artefacts according to Ref. [35] have to be considered. The test cell is provided with gold-coated flow fields on both sides and 1 mm thick titanium fiber PTLs as per scheme, see supplementary information S1. The tested CCM is commercially produced and presents a 120 μm thick membrane with 2.3 $mg \bullet cm^{-2}$ of iridium oxide and 0.35 $mg \bullet cm^{-2}$ platinum on the anode and cathode electrodes, respectively. The measurements were carried out at an in-house built test bench at Fraunhofer ISE, see section Test benches, Fraunhofer ISE test bench 2.

The reference electrode used at Leibniz University Hannover is a salt bridge reference electrode which is incorporated into the 4 cm^2 test cell by Fraunhofer ISE mentioned above. This approach should be able to minimize or even exclude artefacts discussed in Ref. [35]. The salt bridge is integrated through one of the end plates, terminating in the flow field. The other end of the salt bridge is immersed in a 0.5 M sulfuric acid solution. An external reference electrode (Ag/AgCl RE from *Bioanalytical Systems, Inc.*, USA with a 3 $mol \bullet l^{-1}$ NaCl solution) is employed in the same solution. The salt bridge requires humidification during operation to maintain protonic conductivity. Refer to Ref. [7] for a comprehensive overview and a schematic can be found in the supplementary information S2. Regarding salt bridge reference electrode preparation, the PTL undergoes a 15-min ultrasonic bath cleaning, followed by impregnation at the point touched by the salt bridge tip. This impregnation involves applying 1 μL of a 5 wt% Nafion solution. Platinum-coated titanium fiber PTLs are used for both the anode and cathode, along with the standard CCM used in this work. The measurements have been performed at an in-house built test bench at Leibnitz University of Hannover, see section Test benches above.

2.5. PTL impregnation

Since capacitive diffusion processes and the inductive loop appear at similar time constants it is hard to investigate the share of both processes on the total cell resistance. From previous studies it is known that a bad transport of gas in the PTL increases diffusion related resistances since gas molecules block active catalyst parts [15,24,27,29] which can be detected due to additional capacitive processes at low frequencies in impedance spectra. To increase the diffusion resistances, we impregnated the PTL used in one setup of this study with liquid and hardening silicon to impede the gas transport and increase the gas concentration in the catalyst layer on purpose. It is assumed that there is very little impact on water transport by the silicon impregnation compared to the gas transport due to water soaking tests. To ensure electrical contact to the surrounding components (CCM and bipolar plate) the silicon on the PTL surface is grinded and only the inner pores remain blocked. As can be seen in the results, the series resistance of the impregnated PTLs is always higher compared to the measurements with unmodified PTLs. This needs to be attributed to remaining silicon on the PTL surface leading to increased contact resistance. Treating the PTL on the full area was only possible for the cathode. For the anode a drastic increase of mass transport overpotential was observed which exceeded the voltage limit. Therefore, the silicon treatment on the anode PTL was only done for half the area. In all measurements only one PTL is impregnated, the respective other remains unmodified. A commercial CCM is used for these measurements. Pictures of the modified PTLs are given in the supplementary information S3.

2.6. Anode catalyst layer variation

To understand the influence of CCM morphology on the inductive loop, anode catalyst layers with varying iridium oxide particle types and number or printed layers are produced at Fraunhofer ISE using screen printing. The catalyst material is provided by *Heraeus Precious Metals GmbH & Co. KG*, Germany. The cathode catalyst layers and the membrane (FS-990-PK PEM) provided by *Fumatech BWT GmbH*, Germany are the same for each produced CCM.

Two different types of anode catalyst powder which are differentiated in “fine” (mean particle size 1.3 μm) and “coarse” (mean particle size 4.7 μm) are used. The iridium content for both catalyst powders is 83 wt%. All catalyst layers have the same ionomer solid content of

Table 1
CCM properties of Fraunhofer ISE in-house produced CCMs used for anode catalyst layer variation.

CCM	Anode loading/ $mg_{Ir} \bullet cm^{-2}$	Anode IrOx catalyst type	Anode layer no.	Screen mesh count per inch/wire diameter μm	Cathode loading/ $mg_{Pt} \bullet cm^{-2}$
1	0.83 ± 0.05	Fine	1	400/18	0.400 ± 0.007
2	0.736 ± 0.026	Coarse	1	400/18	0.396 ± 0.013
3	0.845 ± 0.015	Coarse	2	520/11	0.404 ± 0.008

16.67 wt% and comparable ink preparation. The catalyst layers are screen-printed on a PTFE decal foil and later transferred by hot pressing onto the membrane. The catalyst loading per print was varied by using different meshes for screen printing.

A summary of the CCMs used in this study is given in Table 1.

2.7. Membrane thickness variation

To investigate the influence of different membrane thicknesses on the inductive loop three different Nafion™ based membranes are used and coated with the same anodic and cathodic catalyst layer at Fraunhofer ISE. The anode catalyst powder is provided by *Alfa Aesar*, USA and the cathode catalyst powder by *Umicore AG & Co. KG*, Germany. The anode has a loading of $(1.10 \pm 0.01)\ mg_{IrO_x} \cdot cm^{-2}$ with 16.67 wt% ionomer and the cathode $(0.50 \pm 0.03)\ mg_{Pt} \cdot cm^{-2}$ with 29.49 wt% ionomer. The iridium content of the anode catalyst particles is 84.5 wt%. The employed membranes are N212™ (50 μm), N115™ (125 μm) and N117™ (178 μm).

2.8. Impedance spectroscopy

A simple method to get information of an electrochemical cell is the polarization curve, where a DC current is applied and the DC voltage is measured. However, this does not allow for a detailed investigation of the ongoing loss processes. Therefore, in this study EIS is used. For further information to this method we refer to Refs. [36–38]. The impedance measurements are performed in galvanostatic mode at different DC bias current densities ranging from 0.5 $A \bullet cm^{-2}$ to 6 $A \bullet cm^{-2}$. The default operation point in this study is at 60 °C and ambient pressure. At KIT the water was supplied only at the anode with a flow rate of 15 $ml \bullet min^{-1} \bullet cm^{-2}$ and at Fraunhofer ISE a flow rate of 25 $ml \bullet min^{-1} \bullet cm^{-2}$ was fed to anode and cathode. An alternating current (AC) with a small perturbation of 10 % of the DC current is applied. The spectra were measured over a frequency range of 100 kHz to 100 mHz with a frequency resolution of 10 steps per decade and an integration time according to 10 periods.

Before the electrochemical characterization a well investigated break-in procedure is performed. For the commercial CCM a voltage of 1.7 V is applied and held for 12 h. For the CCMs prepared at Fraunhofer ISE a specific break-in procedure is done mainly consisting of repeated polarization curves and constant voltage mode for several hours. Before each impedance measurement the stability of the cell is checked regarding the voltage response during a holding time of 5 min at the current DC-bias.

2.9. Kramers-Kronig test

To ensure the data quality of the measured impedance spectra, the Kramers-Kronig test is applied [39]. All measured spectra are checked using the method outlined in Ref. [40]. Importantly, all spectra presented in this work are tested on the Kramers-Kronig relations across the entire frequency range, including the low frequency region of the inductive loop. This accordance to the test is particularly critical when employing the measured data in the Distribution of Relaxation Times (DRT) analysis, which demands exceptional data quality [41]. Even minor deviations or inaccuracies in measurement points can result in misinterpretation of the analyzed data. Therefore, maintaining strict compliance with the Kramers-Kronig test is imperative to ensure the reliability of the findings presented in this study. The Kramers-Kronig residuals for the measurement in Fig. 1 a) are shown exemplarily for all other conducted EIS in this publication in the supplementary information S4.

2.10. Distribution of relaxation time (DRT)

Typically, impedance data are analyzed using an equivalent circuit model, developed with a priori information of an unknown system. The Distribution of Relaxation Times (DRT) method offers an alternative approach, circumventing the need for such prior knowledge. This method enables the identification and deconvolution of polarization processes based on their characteristic time constants, eliminating the necessity for a priori information about the system.

The DRT relies on the approximability of any capacitive system into a series connection of RC elements and a series resistance. By distributing the resistance values of the RC elements over their associated time constants, impedance spectra are transformed into a DRT exhibiting a higher resolution in the frequency domain and thus enabling a deconvolution of processes with close time constants [42].

An impedance Z(ω) and its distribution function g(τ) of relaxation times τ [42] are linked via Equation (1):

$$Z(\omega) = R_0 + R_{pol} \int_0^\infty \frac{g(\tau)}{1 + j\omega\tau} d\tau \quad (1)$$

Here, R_0 represents the ohmic resistance and R_{pol} the polarization resistance of the impedance. To calculate the DRT of the measured spectra, we employed a numerical approach based on fitting, stabilized by the Tikhonov regularization [43,44]. To choose the optimal value for the regularization parameter is challenging, since low values can lead to an overestimation of the number of processes and high values might not properly resolve processes with close time constant. Therefore, we analyzed the impedance data using DRT with different values for the regularization parameter shown in S5 (supplementary information) for the measurement of Fig. 1 at 3 $A \bullet cm^{-2}$. A value of $\lambda = 0.0001$ clearly shows too many peaks which cannot be attributed to physico-chemical processes, $\lambda = 0.01$ showed a logical number of peaks but cannot properly resolve the charge transfer region. Performing this analysis for a number of impedance spectra measured at varied operating conditions, we found the optimal value for our measurements to be $\lambda = 0.005$. This result is also in good agreement with the values used for PEM fuel cell studies [45] with our approach being slightly more conservative to minimize misinterpretation.

Typically, the DRT accounts only for capacitive processes, considering positive resistance and time constant values. To include inductive effects is challenging as they are represented by negative values in the DRT. Enabling negative and positive values simultaneously creates problems regarding the numerical DRT calculation and adaptations in the procedure are necessary. This observation was made by Schiefer et al. [17] at KIT IAM-ET working in the field of PEM fuel cells. They developed an adaptation of the DRT calculation to display the inductive part, allowing for negative resistance and capacity values in defined parts of the spectrum. This adaptation proved meaningful as it demonstrated a physicochemical resistance decay correlated with an increase in current density. The current-related resistance decay corresponds to a gradual reduction of an ohmic or polarization resistance contribution [16]. The inductive process consequently leads to a delayed improvement in cell performance, with the delay time corresponding to the relaxation frequency of the process. For further details on the adaptation of the DRT, we refer to Schiefer et al. [17].

2.11. Equivalent circuit modeling

To analyze and interpret impedance-based measurements, equivalent circuit modeling (ECM) is a widely used approach [36–38]. Ohmic, kinetic and mass transport related contributions can herewith be separated and quantified. Directly applying ECM on EIS requires a fundamental knowledge on the electrochemical processes happening in the cell. For the here discussed inductive loop there is yet no physical model suggested in PEM water electrolysis. Referring to PEM fuel cells, different electrochemical models for inductive loops are reported. Gerling et al. [18] present a numerical simulation model to analyze the change of platinum and platinum oxide state at the oxygen reduction reaction (ORR) in the catalyst layer. Göhr and Schiller [46] present a fundamental use of the relaxation impedance changing with a potential-depending time constant which is sensitive to changes of the structure and properties of the catalyst surface and the formation of the double layer capacitance. This model is used by Schiller et al. [47] to describe a carbon monoxide poisoning of the catalyst layer for the hydrogen reduction reaction (HRR).

If the physical understanding of certain processes is missing, the DRT can provide a spectrum of the polarization processes over the frequency. This allows to understand how many relevant processes are to be considered. In a first attempt each peak in the DRT is modelled by a RQ-elements consisting of a resistance in parallel to a constant phase element (CPE). The resulting equivalent circuit model (ECM) is fitted to the impedance spectra applying a complex non-linear least squares (CNLS) fit.

For the inductive process at low frequencies and their “negative” resistance magnitude, we here allow negative resistance and capacitance respectively CPE values. At first glance these negative values seem to be not physically meaningful. This is not the case considering coupled physicochemical processes in the cell that exhibit a current voltage relation corresponding to a negative resistance/capacitance.

2.12. Overview of performed measurements

In Table 2 the performed measurements discussed in this paper are summarized and essential information are given. More detailed information on catalyst layer and membrane used for the at Fraunhofer ISE produced CCMs can be found in the respective sections.

3. Results

3.1. Inductive effects in impedance spectra and VI scans

The data presented in the manuscript are openly available [48]. To investigate the inductive effect a current density variation was performed at Fraunhofer ISE shown in Fig. 1 a) in the Nyquist and Fig. 1 b) in the respective DRT representation. Looking at the Nyquist plot, at low current densities no inductive loop is visible, but clearly increasing with increasing current density. At 6 $A \bullet cm^{-2}$ the capacitive and inductive polarization is very equal in magnitude and so the high frequency series resistance is very comparable with the resistance at 100 mHz which is close to the direct current resistance detectable from polarization curve measurements. For more information on the comparison to polarization curve measurements we refer to our previous work [21]. At high frequencies (>30 kHz) inductivities are detectable which can be related to wiring issues.

Focusing on the DRT plot it can easily be seen that the inductive loop is increasing with increasing current density with a shift in frequency between 0.2 Hz and 2 Hz. The large capacitive loop which can be related to the anodic charge transfer resistance is decreasing with a shift towards higher frequencies from 60 Hz to 800 Hz. Between 20 Hz and 100 Hz an additional peak gets visible with increasing current density which might be related to transport processes. At frequencies around 1000 Hz a process which is decreasing with current density is detectable which might be related to the comparably low charge transfer resistance of the cathode. At frequencies $> 10^4$ Hz there are further peaks visible, but the data cannot be analyzed due to cable inductivities.

Additional to this, we present a fundamental use of equivalent circuit modeling (ECM) with negative RQ-elements to quantify the polarization magnitude of the inductive loop. Fig. 1 c) shows the ECM for our RQ-element approach discussed in *Experimental* and Fig. 1 d) the fitting results for a current density of 3 $A \bullet cm^{-2}$. The fit shows a very good agreement with the impedance measurement at low frequencies which is clearly the focus of this publication. In the frequency range of charge transfer resistance (100 Hz–1000 Hz) the fit quality is suitable. For higher frequencies small deviation are occurring which could be related

Table 2
Overview of the performed measurements and used equipment.

Figure	Test bench	Test cell	CCM	PTL	Target of measurements
1	Fraunhofer ISE test bench 1	Fraunhofer ISE 4 cm^2 cell	Commercial CCM 1	Commercial PTLs	Analyze impact of current density
2	Greenlight Innovation Test Bench at KIT	Fraunhofer ISE 4 cm^2 cell	Commercial CCM 1 & Fraunhofer ISE CCM (high mass transport)	Commercial PTLs	Comparison of impedance with DC measurements
3	Greenlight Innovation Test Bench at KIT	Fraunhofer ISE 4 cm^2 cell	Commercial CCM 1	Commercial PTLs	Sensitivity analysis of operational parameter
4 a) and b)	Fraunhofer ISE test bench 2	Fraunhofer ISE 23 cm^2 cell with reference electrodes	Commercial CCM 2	Commercial PTLs	Separation of anode and cathode impedance
4 c) and d)	Leibnitz University Hannover test bench	Fraunhofer ISE 4 cm^2 cell with reference electrodes	Commercial CCM 1	Commercial PTLs	Separation of anode and cathode impedance
5	Fraunhofer ISE test bench 1	Fraunhofer ISE 4 cm^2 cell	Commercial CCM 1	Commercial PTLs	Analyze cell with increased mass transport resistance
6	Greenlight Innovation Test Bench at KIT	Fraunhofer ISE 4 cm^2 cell	ISE CCM produced for anode catalyst layer variation	Commercial PTLs	Analyze impact of different anode catalyst layer proerties
7	Greenlight Innovation Test Bench at KIT	Fraunhofer ISE 4 cm^2 cell	ISE CCM produced for membrane thickness variation	Commercial PTLs	Analyze impact of different membrane thicknesses

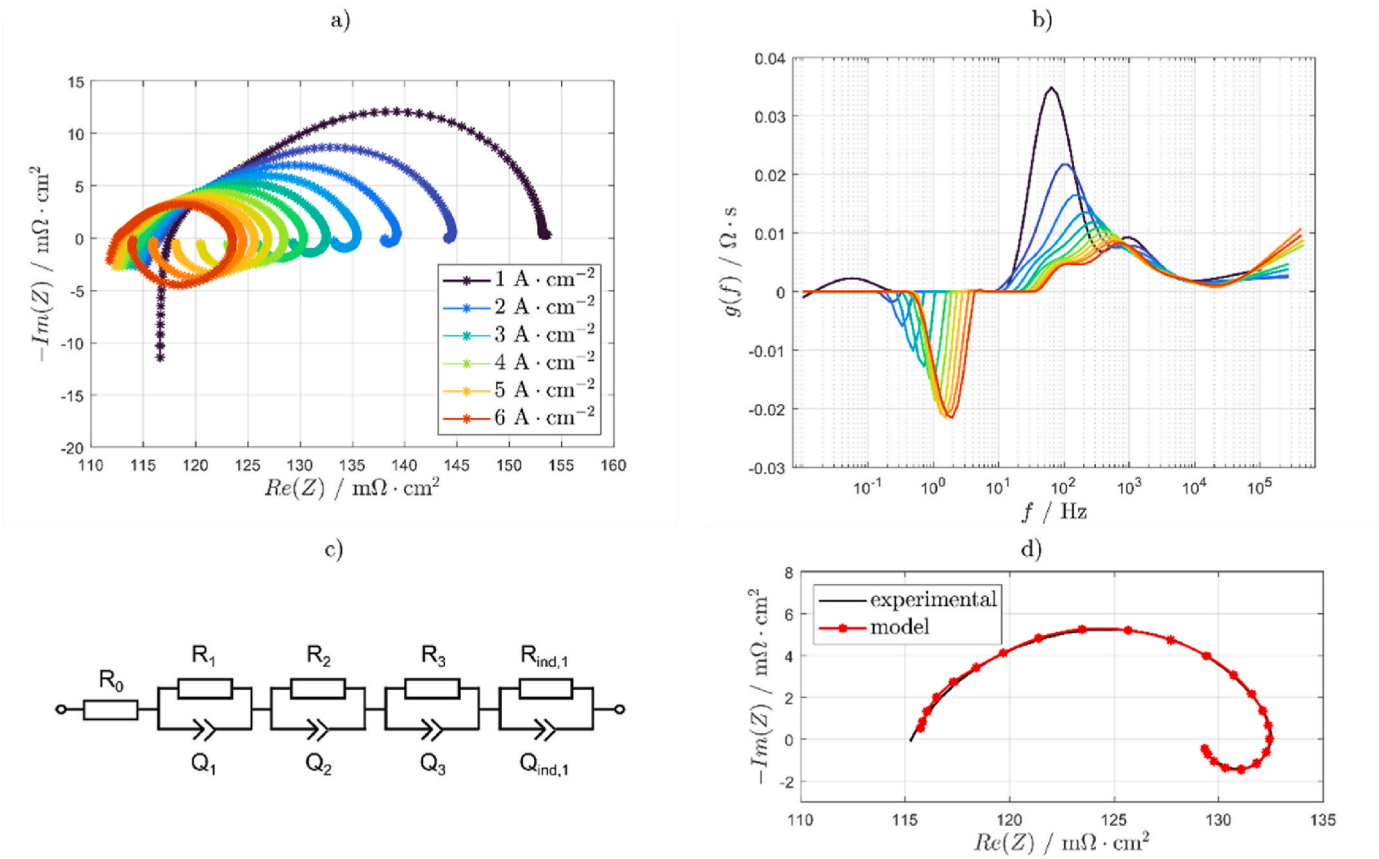

Fig. 1. a) Nyquist presentation of a current density variation, b) DRT analysis including inductive part, c) equivalent circuit model (ECM) with RQ-elements and d) ECM fit results at 3 A•cm−2 for ECM from c).

to the influence by wiring on the measurement and the fact that we do not use an inductance element in our model.

To prove that the inductive loop is not only observable in impedance spectra but also influences the cell performance in DC measurements, voltage current scans (VI scans) with different scan rates between 1000 mV•s^{-1} and 10 mV•s^{-1} were performed. The VI scans as well as DRTs.

- of the commercial CCM with low mass transport losses and
- an ISE in-house CCM designed for high mass transport losses

Are displayed in Fig. 2 a) and b), respectively.

In case of the commercial CCM large inductive loops increasing with increasing current density are observed at f < 10 Hz. In case of the cell with high mass transport losses no inductive features are visible. Instead, there are large capacitive contributions in the DRT related to the mass transport losses. It cannot be excluded that the inductive contributions exhibiting a negative resistance and DRT values exist in this cell as well. In this case the DRT reveals the sum of negative and positive contributions.

Concerning VI scans, usually a higher scan rate shows a better performance since capacitive low frequency processes are too slow to contribute to the measured VI scan. We therefore started with a scan rate of 1000 mV•s^{-1} which corresponds to a scan duration of 800 ms for the commercial CCM and 600 ms for the ISE in-house CCM. The difference in scan duration is due to the different voltage response of the two CCMs (commercial CCM ~2.3 V and ISE in-house CCM ~2.1 V at 5 A•cm^{-2}), which is mainly coming from the different membrane thicknesses of 125 μm and 90 μm, respectively. To be able to compare it to the time scale of the different processes we included a second x-axes in the DRT to show which processes are not included in the fast scan rates. The correlation between the frequency f applied in the EIS and the time constant of the processes τ are given in Equation (2). As can be seen, a scan duration of 800 ms or 600 ms do not include all low-frequency processes. However, with decreasing scan rate more relevant low-frequency processes are included in the VI scan measurements.

$$\tau = (2 \cdot \pi \cdot f)^{-1} \quad (2)$$

In the low current density region (<3 A•cm^{-2}) of the VI scans for both CCMs it can be seen that the assumption holds true and for both CCMs the performance increases with the scan rate. At higher current densities however, there are differences observable between the two CCMs. For the commercial CCM (Fig. 2 a)), the performance now improves with lower scan rates, whereas the ISE in-house CCM (Fig. 2 b)) shows a similar behavior as at low current densities.

This behavior is aligning with the expectation. For a slower scan rate, processes forming inductive loops lead to a performance increase. At high scan rates (e.g., 1000 mV•s^{-1} and 500 mV•s^{-1}) there is not enough time to activate these processes since their time constants are below the respective scan times. Therefore, no improvement on the performance can be detected.

For the ISE in-house CCM on the other hand the faster scan rates show a better performance in the whole current density region. This is related to the dominating capacitive loss processes in the low frequency region. Their positive resistance contribution to the overall internal resistance of the cell increases with decreasing scan rates. It has to be noted here, that at even lower scan rates and slowly measured polarization curves with several minutes holding time the performance gets better even for the CCM with high mass transport. This is attributed to thermal effects related to internal heating of the cell. The cell temperature increases while operating at higher current for a prolonged time.

With these measurements it is shown that the processes in the cell forming inductive loops in the impedance spectra are also recognizable

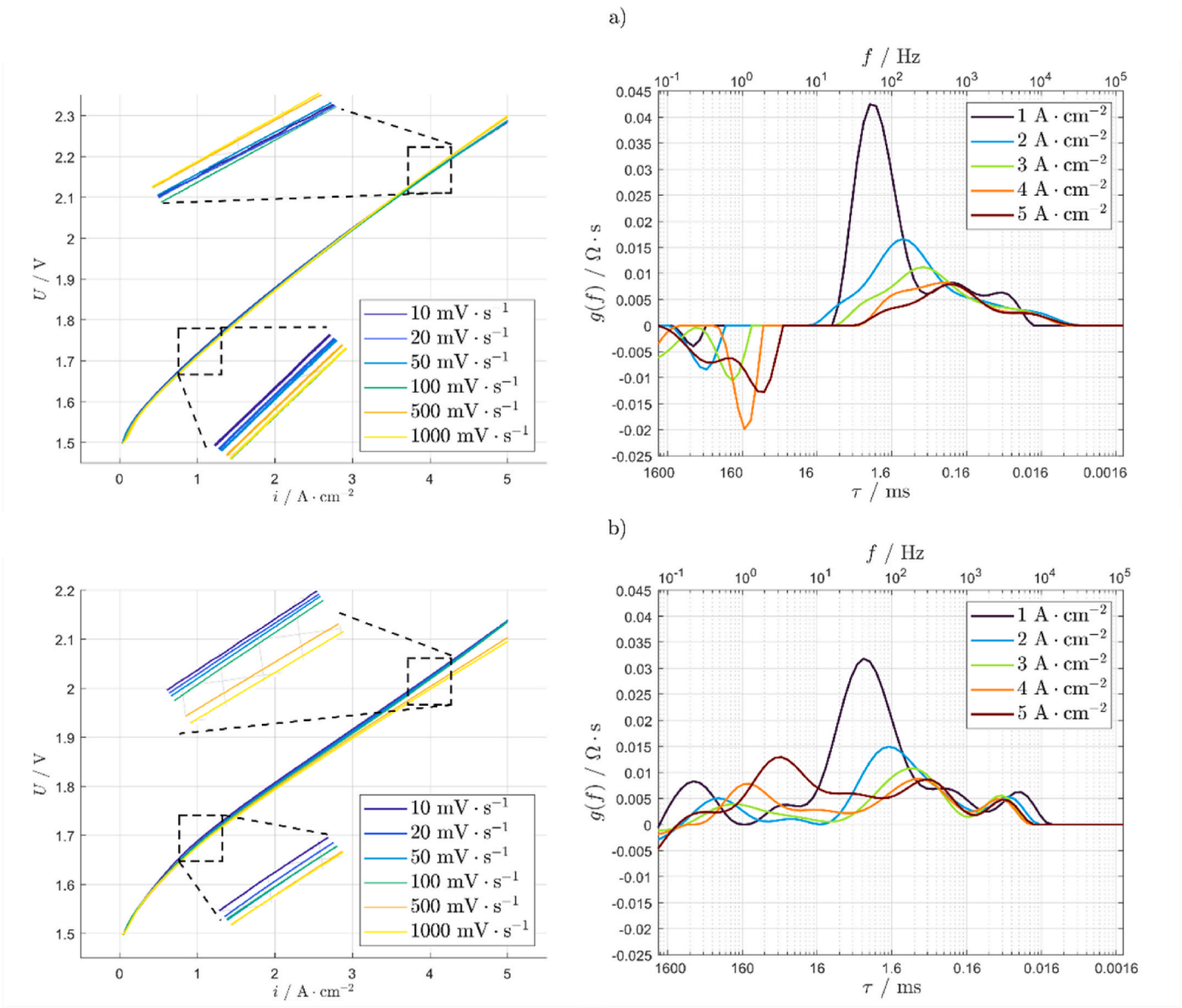

Fig. 2. *VI scans with different scan rates (left side) from* 1000 mV•s^{-1} *to* 10 mV•s^{-1} *with comparison to DRT analysis (right side) of a) commercial reference CCM with high inductive loop and b) ISE in-house CCM with induced high mass transport.*

in DC measurements and lead to an improvement of cell performance. Additional impedance measurements at the same bias current but with varying current amplitude show no effect on the inductive loop, see supplementary information S6. This also hints that the inductive loop is no measurement artefact but related to a physicochemical process in the cell affecting its DC performance.

3.2. Operating parameter variations

To get an overview on the effect of different operating parameters on the inductive loop we performed impedance measurements at different temperatures, pressures, water flow rates (anode side) and current densities. For the flow rate variation, the water flow was decreased in 3.75 ml•min^{-1}•cm^{-2} (15 ml•min^{-1}) steps, starting from 18.75 ml•min^{-1}•cm^{-2} (75 ml•min^{-1}) and going down to 3.75 ml•min^{-1}•cm^{-2} (15 ml•min^{-1}). The results of the last two steps were discarded due to high fluctuations in the temperature.

To compare the size of the inductive loop of each measurement the area specific resistance (ASR) of the inductive part was determined. This was done by fitting the data with the RQ model introduced in section *Impedance analysis*. The results are shown in Fig. 3. The total error related to the accuracy of the measurements and the fitting was determined to be <6 %. The measurement error is mainly related to small fluctuations in temperature and flow rate.

Fig. 3 shows the current density variation with a clear trend visible. With increasing current density and therefore increasing voltage (measured voltages marked in the top x-axis) the negative ASR of the inductive part increases. For the temperature variation, shown in Fig. 3,

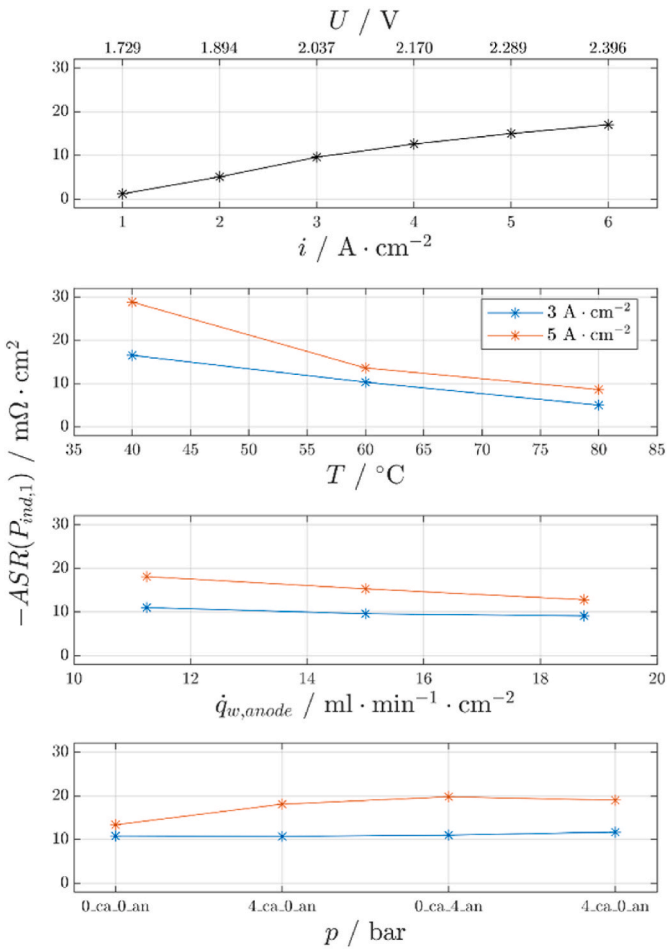

Fig. 3. *Area specific resistance (ASR) values of the inductive part for the following variations from top to bottom: current density variation from* 1 A•cm^{-2} *to* 6 A•cm^{-2}*, temperature variation from 40* °C *to 80* °C*, water flow rate variation from 7.5* ml•min^{-1}•cm^{-2} *to 18.75* ml•min^{-1}•cm^{-2} *and pressures of* 0 barg *to* 4 barg.

a clear trend is visible as well. With increasing temperature, the negative ASR decreases. This behavior might also be associated with the higher voltage occurring at the lower temperature for the same current density. A temperature and current density variation were also performed in our previous work using different setups and materials. For further information on this we refer to our previous study [21]. The flow rate variation as well as the pressure variation show no significant impact on the negative ASR of the inductive loop (Fig. 3). It should be noted here that the water flow rate is comparably high and could not be lowered further due to arising temperature instability at the test rig which we refer to a cooling problem since the test cell is not designed for such low flow rates and has no external heating management implemented. Therefore, the influence of the water flow rate on a stoichiometric level could not be investigated. For PEM fuel cells Meyer and Zhao reported a strong influence of the inlet air flow on the inductive loop. They oscillated the inlet air flow depending on the applied frequency of the AC current density signal during impedance measurements and observed increasing inductive loops [49]. In the measurement shown here, as well as in our previous work [21], we made sure that the inlet water flow is not affecting the impedance measurements. Only chaotic, non-frequency depending deviations occurred due to the mass flow oscillations <1 %. Since the pressure does not show any large and explicit impact on the ASR, it is rather unlikely that the process behind it is related to a process in the gas phase.

3.3. Analysis of anode and cathode via reference electrodes

In Fig. 4 we compare the results of the two cell setups from Fraunhofer ISE (laser ablation reference electrode) and Leibniz University Hannover (salt bridge reference electrode). It is important to underline that the two setups are different in their approach. For the laser ablation reference electrode, we target to split the cell voltage in the center of the membrane (through-plane direction), therefore the ohmic contribution can be seen at anode and cathode and the polarization resistance is divided into anodic and cathodic contributions.

Using the salt bridge reference electrode, we split the cell voltage at the catalyst layers protonic potential, therefore we see most of the ohmic contribution only at the electrode without implemented reference electrode (anode). The voltage at the electrode with the reference electrode only includes minor ohmic resistances. The activation overpotential is separated into its contributions from the anodic oxygen evolution reaction (OER) and the cathodic hydrogen evolution reaction (HER). For both setups it has to be mentioned, that they have uncertainties as discussed by Adler at el [32,35]. and the results have to be regarded with care and are only used to hint in a direction to which side the inductive behavior might be connected. Any quantification by fitting the spectra should be avoided.

Fig. 4 a) and b) show the Nyquist presentation at 80 °C and the DRT of the Fraunhofer ISE reference electrode measurement at 60 °C and a temperature variation between 40 °C and 80 °C, respectively. The measurements conducted with the reference electrode at anode and cathode are excellently consistent. The inductive process at low frequencies is only observable at the anode with two significant peaks at > 0.1 Hz and >1 Hz. In contrast to this we only see capacitive polarization at the cathode which should be related to diffusion processes at these low frequencies. The temperature dependency of the DRT analysis supports this interpretation since the diffusion polarization resistances (<100 Hz) are decreasing with increasing temperature. The change in the high frequency inductive part of the spectra of cathode and full cell might be attributed to the effects described in Ref. [32]. Thus, a part of the inductive behavior at the anode might be related to an effect induced by the reference electrode.

Fig. 4 c) and d) show the results of the salt bridge reference electrode by Leibniz University Hannover introduced in *Experimental*. In Fig. 4 c) the Nyquist representation is shown for the mean cell as well as the anode versus reference and the cathode versus reference. For all these measurements the reference was placed at the cathode side. The cathode impedance shows only capacitive polarization behavior and the anode shows also an inductive contribution at low frequencies. It should be noted here that the measurements of the cathode against reference electrode (orange curve) exhibited Kramers-Kronig residuals with a mean value of 10 % (neglecting the high frequency inductance due to wiring artefacts) most likely due to a bad signal-to-noise ratio.

In Fig. 4 d) the DRT representation for the measurements is shown. As for the Fraunhofer ISE setup, the cathode shows only a capacitive behavior at low frequencies, which might be connected to diffusion processes. The anode on the other hand shows an inductive peak in the low frequency region and also capacitive peaks in the high frequency region.

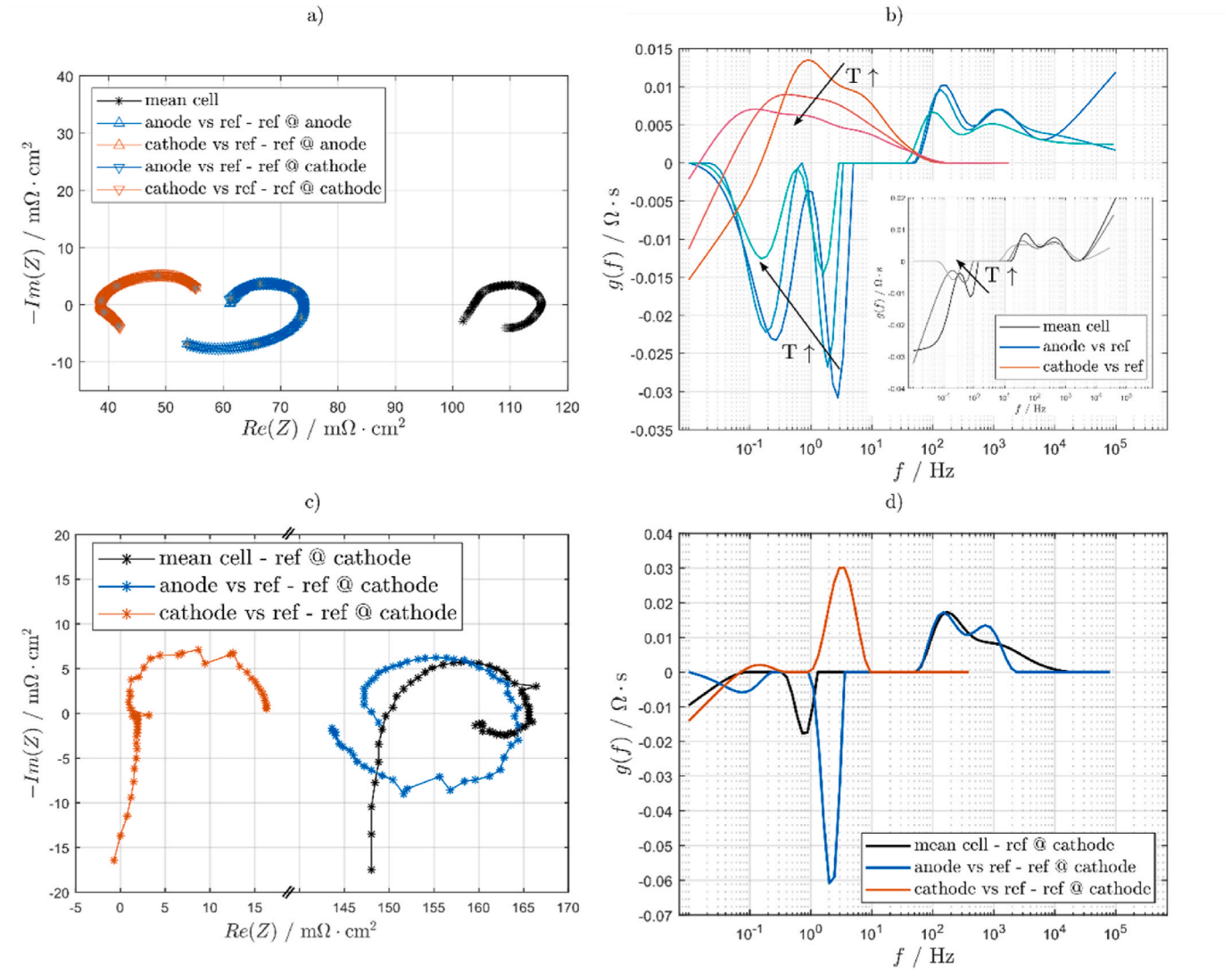

Fig. 4. *Results of impedance measurement with reference electrodes at 4.5* A•cm^{-2} *and ambient pressure. a) Nyquist presentation at 60* °C *and b) DRT analysis of impedance measurements at 40* °C*, 60* °C *and 80* °C *with the Fraunhofer ISE reference electrode setup. c) Nyquist presentation and d) DRT analysis of the reference electrode of Leibniz University Hannover at 60* °C.

These totally different reference electrode setups both show that the inductive loop only occurs at the anode. We did not see any inductive loop contribution from the cathode in all conducted measurements. These results are in consistency with a number of investigations on PEM fuel cells, showing that the low-frequency inductive loop appears at the air electrode [18].

3.4. PTL impregnation

With the silicon impregnation we purposely increase mass transport related polarization resistances at anode and cathode, respectively. This shows the interference between transport related capacitive polarization and the inductive loop. The results of this study are summarized in Fig. 5. Fig. 5 a) shows the polarization curve of the untreated measurement (default setup, black) and the silicon impregnated PTLs at anode (blue) and cathode (orange). The respective other half cells each remained untreated. Even by focusing on DC measurements only, differences in ohmic resistance (steeper linear slope at low current densities) and mass transport resistances (order >1 of the polarization curve at higher current densities) are observable when comparing the not impregnated setup to the impregnated ones, with the anode impregnation showing the strongest impact. To compare the results in more detail the DRT as well as the Nyquist presentation are given in Fig. 5b–d) showing the not impregnated setup, the cathode impregnation and the anode impregnation, respectively.

The Nyquist presentation reveals an increase of ohmic resistance for the impregnated setups with increasing current density. Usually, with increasing current density the series resistance decreases due to temperature increase of the CCM which can be seen for the setup without impregnation in Fig. 1a). We assume that the blocked gas at the interface of catalyst layer (CL) and the PTL occupies contact points and therefore increases the contact resistance with increasing amount of gas at higher current densities. For the anode impregnation (Fig. 5 d)) a second capacitive semicircle as well as an extra peak in the DRT at lower frequencies can be seen which is increasing with current density. The comparison with the Nyquist presentation of the untreated setup (Fig. 5 b)) reveals that the inductive loop cannot be seen as it is superimposed by anodic mass transport polarization. Current densities above 3 A•cm^{-2} were too unstable to conduct EIS for the impregnation of the anode PTL.

In contrast to this, the impregnation at the cathode (Fig. 5 c)) shows that the mass transport at the cathode occurs at higher frequencies (between 1 Hz and 20 Hz, shifting to higher frequencies with current density) and is less interfering with the inductive loop, see zoom in at 3

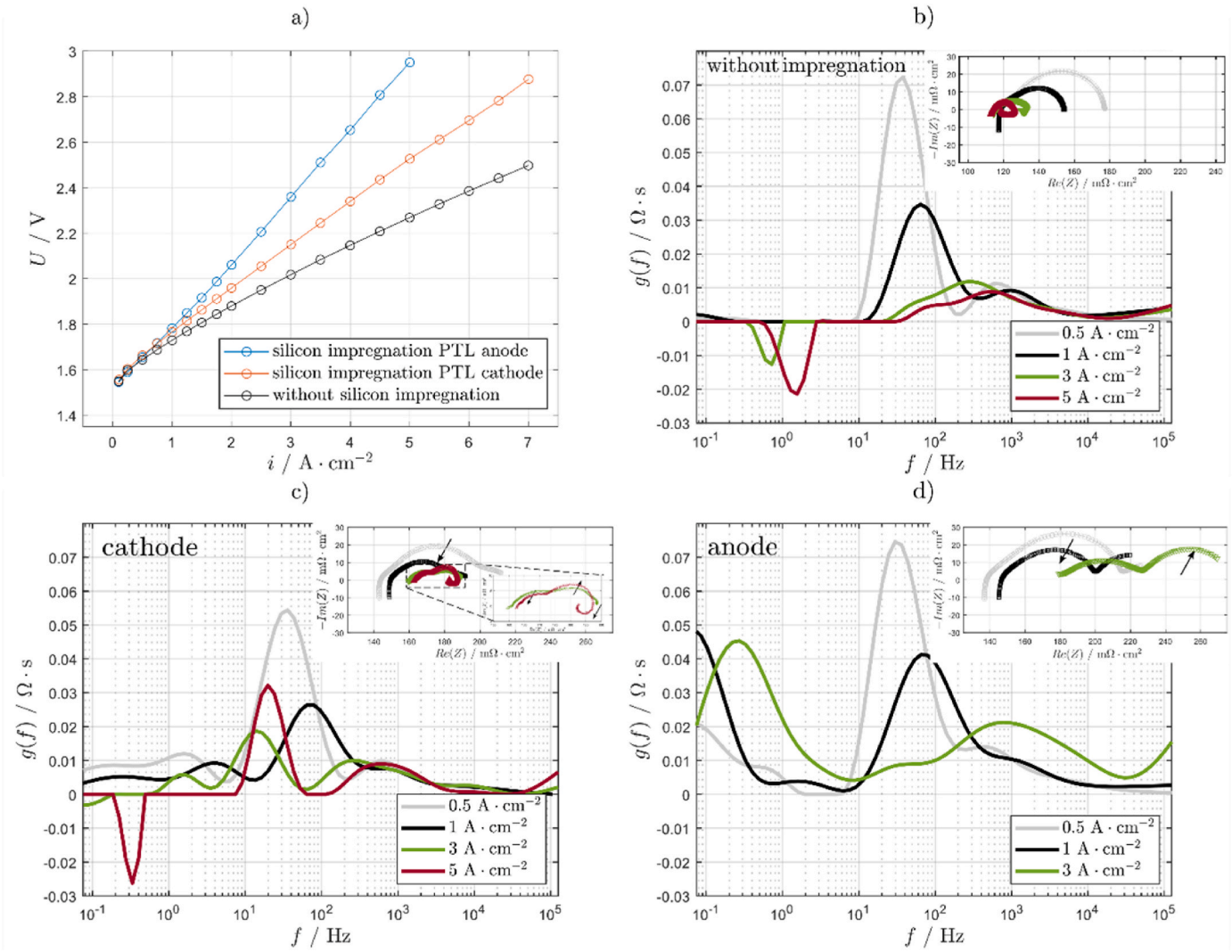

Fig. 5. Silicon impregnation of PTLs at the default operation point. a) Polarization curve of silicon impregnated setups at anode and cathode and the reference without PTL treatment. DRT and EIS presentation at different current densities b) untreated, c) cathode impregnation and d) anode impregnation. (For interpretation of the references to colour in this figure legend, the reader is referred to the Web version of this article.)

A•cm^{-2} and 5 A•cm^{-2} in Fig. 5 c). While the peak at ~40 Hz (most-likely related to charge transfer) is decreasing with current density, both the capacitive (mass transport related) and the inductive loop are increasing. The DRT analysis (Fig. 5b–d)) show clearly that the anodic transport polarization is happening at very similar frequencies as the inductive loop (between 0.1 Hz and 0.5 Hz). The cathode diffusion peak appears slightly higher than the inductive loop of the untreated setup between 1 Hz and 2 Hz and is not directly superimposing the inductive loop. The capacitive peak at 10 Hz is also significantly increased compared to the untreated setup which might also be related to a cathodic transport process. It should be noted that at higher frequencies (>10^2 Hz) also the charge transfer process is influenced by the silicon treatment of the PTLs. We assume that this is related to lower electrical and ionic contacting due to silicon which remains on the PTL surface. This also explains why the silicon treatment at the anode has a higher influence at these frequencies since the kinetic overpotentials are usually more relevant compared with the cathode. Herewith, we can show that with increasing current density besides the inductive also the mass transport polarization is increasing and that the inductive process is strongly depending on the anode side which is consistent with the reference electrode measurements.

3.5. Anode catalyst layer variation

With a variation of anode catalyst layer, we want to understand the influence of structural properties on the low-frequency inductive behavior. Fig. 6 shows the DRT analysis of the different CCMs listed in Table 1. Fig. 6 a) and b) compare CCMs with similar iridium oxide loading at a current density variation. The anode catalyst layers in CCM 1 and CCM 2 were printed with one layer, with CCM 1 employing fine particles and CCM 2 coarse particles. Additionally, in Fig. 6 c) CCM 3 is shown with coarse particles, comparable loading as CCM 1 and CCM 2, but was produced printing two catalyst layers on top of each other.

CCM 1 shows decreasing resistance contributions at frequencies ~100 Hz with increasing current density which can be related to charge transfer. An increasing resistance contribution with increasing current density is visible at frequencies between 5 Hz and 10 Hz which we would assign to anodic mass transport polarization. At frequencies <1 Hz a second smaller capacitive loop is detectable for CCM 1 which is not increasing with current density, instead seemingly decreasing. Over the whole low-frequency range, no inductive process is detectable at all. CCM 2 on the other hand shows very comparable behavior to our commercial reference cell (see Fig. 1). The charge transfer resistance (~100 Hz) is decreasing and the inductive loop (<3 Hz) is increasing with increasing current density. All CCMs in this study contain the same

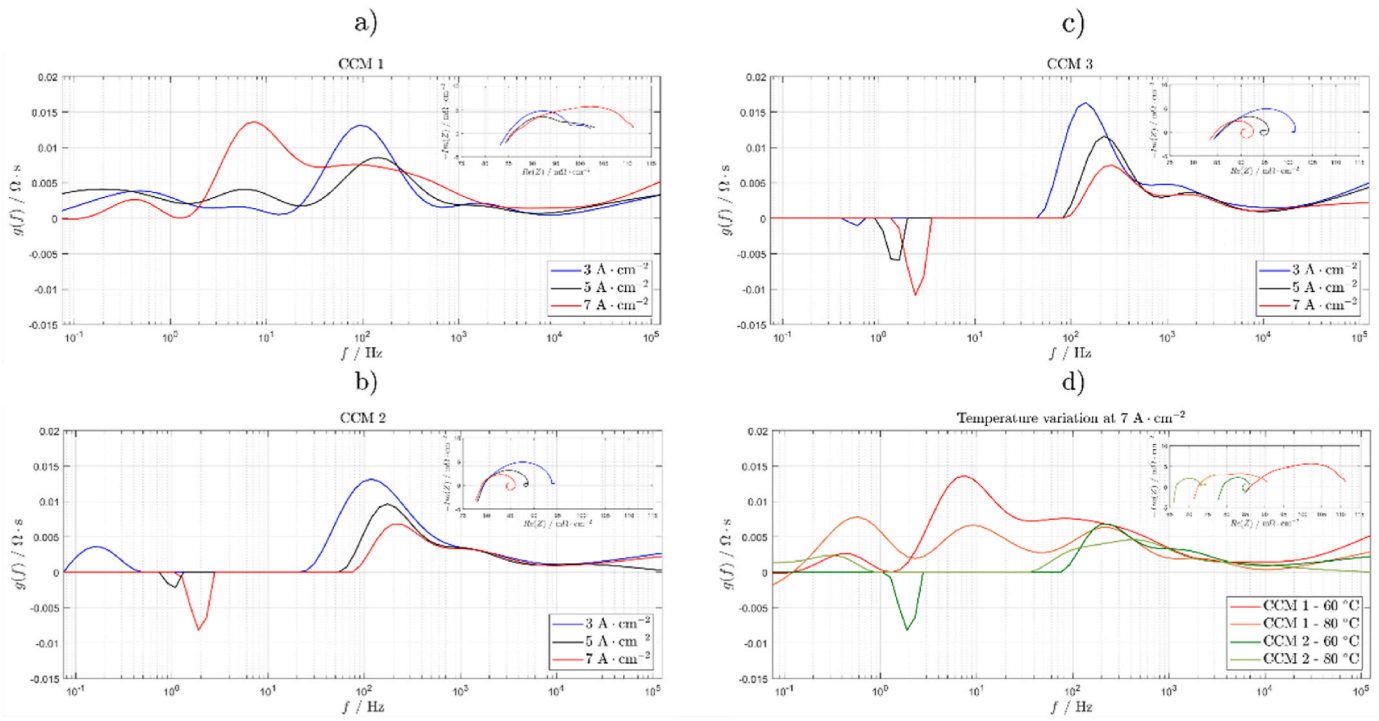

Fig. 6. Comparison of DRT analysis and Nyquist presentation of the CCMs used for catalyst layer variation study, for an overview of the CCMs see Table 1 a) CCM 1, b) CCM2 and c) CCM 3 during a current density variation. d) Temperature variation of CCM 1 and CCM 2.

ionomer to catalyst ratio of 0.2. We believe that due to the different particle sizes the ionomer binds differently to the iridium oxide particles surface leading to a significant variation in the ionomer and catalyst distribution within the catalyst layer. The fine particles (CCM 1) show a significant higher surface area than the coarse particles (CCM 2 and 3) which might enable a better binding of the ionomer leading to a denser packed catalyst layer by ionomer. This could result in the pores being more blocked for CCM 1 compared with CCM2 and 3 and therefore the produced gas requires a higher capillary pressure to get out of the catalyst layer, resulting in increased mass transport resistance. The seemingly decreasing capacitive behavior of CCM 1 at < 1 Hz shows that the inductive process (increasing with current density and therefore reducing the capacitive polarization) is still existing but superimposed by the capacitive mass transport. Comparing CCM 2 with CCM 3 supports this analysis. Both CCMs have an equal loading but CCM 3 has two printed layers, therefore it is less dense packed resulting in less mass transport polarization and larger inductive loops at the same current density.

Fig. 6 d) shows the temperature impact for 60 °C and 80 °C at 7 A•cm^{-2} for CCM 1 and CCM 2. Decreasing temperature leads to increasing inductive behavior (see Fig. 3) which is in this case clearly visible for CCM 2. In contrast to this, CCM 1 shows higher capacitive polarization at ~100 Hz at low temperatures which is consistent with the higher (cathodic) mass transport related polarization behavior at lower temperature, see Fig. 4 b). At < 1 Hz lower capacitive polarization is visible at low temperatures. This again proofs the assumption, that the inductive loop is still existing but not detectable in the impedance measurement since it is superimposed by the mass transport polarization.

With this study we cannot answer the question, whether a denser packed catalyst layer has an impact on the inductive loop or if it is just superimposed by higher mass transport resistance. We can only show that the superimposing of (capacitive) mass transport polarization and the inductive loop is a relevant fact and highly sensitive on anodic catalyst layer properties.

3.6. Membrane thickness variation

To investigate if the thickness of the membrane has an impact on the inductive loop, we performed tests on cells with three different membrane thicknesses but the same anode and cathode catalyst layer. To analyze the impact of the membrane, we performed current density variations and compared the results for the different membranes. At the same current density, we saw quite different inductive loop sizes as presented in Fig. 7 free of high frequency series resistance, exemplarily shown at 5 A•cm^{-2} in Nyquist (Fig. 7 a)) and DRT (Fig. 7 b)) presentation. Since we were facing artefacts at high frequencies all impedance data above 30 kHz is removed. A strong dependency of the inductive loop to the membrane thickness is visible, where the thickest membrane shows the largest loop. As to be expected, the capacitive polarization phenomena at the electrodes are not affected by the membrane and a very good reproducibility of the electrodes regarding charge transfer and mass transport behavior is achieved despite of the different membranes.

What can also be seen from the measurement depicted in Fig. 7 is, that for the thickest membrane the inductive loop compensates the capacitive polarization processes complete and therefore leads to a negative DC resistance while excluding the high frequency resistance. The latter finding might suggest that the inductive loop is related to the membrane as otherwise the electrodes in total would exhibit a negative

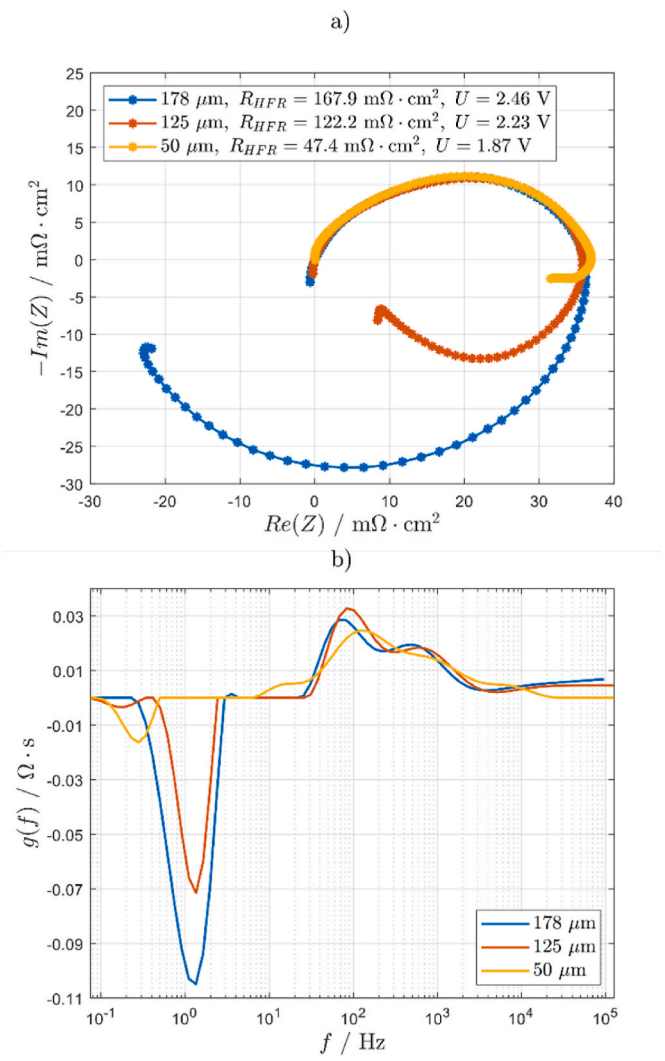

Fig. 7. Membrane variation measurements shown in a) high frequency series resistance (HFR) free Nyquist and b) DRT presentation for EIS at 5 A•cm−2.

resistance. Anyhow it has to be considered that the impedance only represents the differential resistance in the working point. As the electrode polarization is strongly nonlinear, the total polarization resistance of the electrodes at higher current densities is significantly larger than the polarization resistance measured by EIS.

4. Discussion

With the conducted measurements we can encircle the origin and explain structural and operational parameter dependencies of the inductive loop. In Table 3 we list the variations we have performed in this study and give an overview on their impact on the inductive loop as well as possible explanations.

On the operation parameter side, we have varied the current density, temperature, pressure and the water flow rate on the anode side. From these we see that the inductive behavior is affected by current/voltage as well as temperature. It should be noted here that the observed temperature effect might also be connected to the changed voltage at different temperatures due to increased membrane resistance. The pressure and water flow rate show no impact on the inductive loop. Furthermore, we tested two setups with different types of reference electrodes from which we can conclude that the inductive loop seems to be located at the anode side. In the reference electrode measurements and as well in some full cell measurements two inductive peaks are detectable in the DRT. This might hint that there is more than one physicochemical process contributing to the low-frequency inductive features. This is consistent with the findings for PEM fuel cell [17].

Table 3
Parameter variations performed in this study with impact description and possible reasons.

Variation	Observation	Possible Reasons
Current density	Larger loop at higher current/ voltage	• Membrane effect • Anode catalyst
Temperature	Larger loop at lower temperature	• Membrane effect • Anode catalyst
Pressure	No impact	–
Water flow rate	No impact	–
Cathode, anode via reference electrode	Only anode spectra with inductive loop	• Membrane effect • Anode catalyst
PTL impregnation	Strong dependency to anode	• Mass transport overlap
Anode catalyst variation	Larger loop with coarse particles due to less mass transport	• Mass transport overlap
Membrane variation	Larger loop with thicker membrane	• Membrane effect

The PTL impregnation measurements show that there is an overlapping happening between inductive behavior and mass transport losses. If the mass transport losses are increased, the inductive loop is reduced and might even completely vanish. This phenomenon can also be seen in the anode catalyst layer variation with less dense packed catalyst layer due to coarse particles showing less mass transport and therefore a larger inductive loop. This feature leads to a general problem in applying impedance spectroscopy to PEM water electrolysis cells. If two processes with negative and positive resistance contributions are overlapping in their frequency range, they cannot be properly resolved by impedance spectroscopy or any other kind of dynamic measurement.

The membrane thickness variation showed an increased inductive loop with increasing membrane thickness. This finding suggests that an effect inside the membrane is creating the low frequency inductive behavior.

These results allow us to present and rate hypotheses which could explain the inductive processes. Regarding PEM fuel cells three effects are reported: Platinum oxide effects, reaction intermediates and ionomer humidification [18,50]. It has to be mentioned, that PEM fuel cells are significantly different compared with PEM water electrolysis cells. They strongly differ in used cell components and the way of operation (for example reactant stoichiometry). Therefore, a direct transfer of the hypotheses has to be viewed critically. Further investigations on the specific hypotheses are strongly suggested. We believe that ionomer humidification from product water is hardly transferable to our case since we always have a high water to gas ratio in the test cells and therefore the water supply to ionomer is ensured. Also, we did not notice any difference when supplying water to the anode and cathode or the anode only. Local phenomena due to water consumption and gas production at a certain catalyst particle are conceivable but with increasing current density the water amount should decrease at the catalyst and therefore show increasing resistance instead of decreasing. But still, we see a strong impact from the membrane thickness. One explanation for this could be, that due to the electroosmotic drag coupled with slow water diffusion the membrane gets internally way more humidified as only by supplying water to it. This could explain, why the inductive process is increasing with increasing current density (increasing proton transfer through the membrane) and with decreasing temperature. Since the lower the temperature the higher the membrane resistance, a better humidification could in this case be more sensitive. Additionally, it should be considered, that at high current densities the local temperature of the anode catalyst layer could be significantly higher due to the heat dissipation of the reaction. It might be the case that the water

permeating in and through the membrane and ionomer has a higher temperature as the feed water and therefore amplify the resistance decrease at low frequencies.

The other two effects reported in PEM fuel cells, platinum oxide effects and reaction intermediates, are both related to electrochemical phenomena at the catalyst surface. Both are potential driven and would lead to a larger inductive loop at higher voltages, which would be in consistency with our findings. Transferred to the PEM electrolysis case and with keeping our findings in mind, that the inductive loop is coupled with the anode side, a similar hypothesis could be the change of iridium oxidation states with the voltage. Hrbek et al. [51] measured the iridium oxidation state during PEM water electrolysis operation with varying voltages. They show that when changing the operation point between 2 V down to open circuit voltage (OCV) and then up to 2.5 V a reduction of iridium oxide to Ir^0 (iridium black) can occur among the usual states during operation of Ir^{+4} and Ir^{+6}. The change of the iridium oxidation state could lead to a change of the activity and electrical conductivity of the catalyst layer with a certain (comparably slow) time constant which might explain the decreasing resistance at low frequencies. But we hardly believe that a change of the state of iridium due to a voltage change in the mV range can explain that the low-frequency inductive polarization completely compensates the capacitive polarization and leads to a low frequency resistance being smaller than high frequency series resistance. However, it cannot be excluded that it contributes to the low-frequency inductive features.

Further measurements are suggested to be done, like variation of the water flow rate at the anode on stoichiometric level, high differential pressure and detailed variation of structural membrane and anode catalyst properties. To get a better understanding of the chemico-physical process electrochemical and fluid dynamic based modeling is suggested.

5. Conclusion

This study delves into the inductive low frequency processes within impedance spectra of PEM water electrolysis cells. From the measurements conducted in this study, we come to the following statements which should still be considered with caution and not seen as a final answer:

Inductive effects at low frequencies.

- affect the DC performance of the cell and are visible in DC measurements
- are not affected by the EIS amplitude
- are not affected by water flow rate and pressure change in the regions varied in this study
- are strongly affected by temperature and current density/voltage
- are only observable in the spectra of the anode
- can overlap with low frequency mass transport processes
- are strongly influenced by membrane thickness

From our investigation and with the knowledge from PEM fuel cells we could give some possible origins of the inductive loop. One possible explanation is a membrane humidification effect. Another reason might be changing iridium states, but we do not believe that this could be the only reason for the inductive loop. Since we see two inductive peaks in the DRT of some measurements there could also be more than one effect in play. There is also a strong interaction with the mass transport losses especially on the anode side and therefore it is challenging to separate mass transport related polarization and inductive effects in impedance spectra or other dynamic measurements as CVs.

CRediT authorship contribution statement

Debora Brinker: Writing – original draft, Visualization, Validation, Project administration, Methodology, Investigation, Formal analysis, Conceptualization. **Niklas Hensle:** Writing – original draft, Visualization, Validation, Project administration, Methodology, Investigation, Formal analysis, Conceptualization. **Jerónimo Horstmann de la Viña:** Writing – review & editing, Investigation, Conceptualization. **Irene Franzetti:** Writing – review & editing, Investigation, Conceptualization. **Lena V. Bühre:** Writing – review & editing, Investigation. **Umesh Anirudh Andaluri:** Investigation. **Charlotte Menke:** Investigation. **Tom Smolinka:** Writing – review & editing, Supervision, Funding acquisition, Conceptualization. **André Weber:** Writing – review & editing, Supervision, Funding acquisition, Formal analysis, Conceptualization.

Declaration of competing interest

The authors declare that they have no known competing financial interests or personal relationships that could have appeared to influence the work reported in this paper.

Data availability

The data presented in the manuscript are openly available in the KITopen repository at DOI: 10.35097/KUsZkubcrDwyvyjm

Acknowledgment

D. Brinker and N. Hensle contributed equally to this publication. The authors gratefully acknowledge funding from the Federal Ministry of Education and Research, Germany (BMBF 03HY103C and 03HY103F) and the Federal Ministry for Digital and Transport, Germany (BMDV 03B11018A). We thank Schaeffler Technologies AG & Co. KG, Germany and Heraeus Precious Metals GmbH & Co. KG, Germany for the collaboration.

Appendix A. Supplementary data

Supplementary data to this article can be found online at https://doi.org/10.1016/j.jpowsour.2024.235375.

References

[1] J. van der Merwe, K. Uren, G. van Schoor, D. Bessarabov, Characterisation tools development for PEM electrolysers, Int. J. Hydrogen Energy 39 (26) (2014) 14212–14221, https://doi.org/10.1016/j.ijhydene.2014.02.096.
[2] M. Suermann, A. Pătru, T.J. Schmidt, F.N. Büchi, High pressure polymer electrolyte water electrolysis: test bench development and electrochemical analysis, Int. J. Hydrogen Energy 42 (17) (2017) 12076–12086, https://doi.org/10.1016/j.ijhydene.2017.01.224.
[3] S. Siracusano, S. Trocino, N. Briguglio, V. Baglio, A.S. Aricò, Electrochemical impedance spectroscopy as a diagnostic tool in polymer electrolyte membrane electrolysis, Materials 11 (8) (2018), https://doi.org/10.3390/ma11081368.
[4] J.C. Garcia-Navarro, M. Schulze, K.A. Friedrich, Measuring and modeling mass transport losses in proton exchange membrane water electrolyzers using electrochemical impedance spectroscopy, J. Power Sources 431 (2019) 189–204, https://doi.org/10.1016/j.jpowsour.2019.05.027.
[5] I. Dedigama, P. Angeli, K. Ayers, J.B. Robinson, P.R. Shearing, D. Tsaoulidis, et al., In situ diagnostic techniques for characterisation of polymer electrolyte membrane water electrolysers – flow visualisation and electrochemical impedance spectroscopy, Int. J. Hydrogen Energy 39 (9) (2014) 4468–4482, https://doi.org/10.1016/j.ijhydene.2014.01.026.
[6] I. Franzetti, A. Pushkarev, A.-L. Chan, T. Smolinka, Parasitic effects in impedance spectrum of PEM water electrolysis cells: case study of high-frequency inductive effects, Energ. Tech. (2023), https://doi.org/10.1002/ente.202300375.
[7] L.V. Bühre, S. Bullerdiek, P. Trinke, B. Bensmann, A.-L.E.R. Deutsch, P. Behrens, et al., Application and analysis of a salt bridge reference electrode setup for PEM water electrolysis: towards an extended voltage loss break down, J. Electrochem. Soc. 169 (12) (2022) 124513, https://doi.org/10.1149/1945-7111/ac9ee1.
[8] C.C. Weber, T. Schuler, R de Bruycker, L. Gubler, F.N. Büchi, S de Angelis, On the role of porous transport layer thickness in polymer electrolyte water electrolysis, Journal of Power Sources Advances 15 (2022) 100095.
[9] T. Schuler, C.C. Weber, J.A. Wrubel, L. Gubler, B. Pivovar, F.N. Büchi, et al., Ultrathin microporous transport layers: implications for low catalyst loadings, thin membranes, and high current density operation for proton exchange membrane electrolysis, Adv. Energy Mater. (2024).

[10] M. Rogler, M. Suermann, R. Wagner, S. Thiele, J. Straub, Advanced method for voltage breakdown analysis of PEM water electrolysis cells with low iridium loadings, J. Electrochem. Soc. 170 (11) (2023) 114521, https://doi.org/10.1149/1945-7111/ad0b74.
[11] Z. Kang, S.M. Alia, J.L. Young, G. Bender, Effects of various parameters of different porous transport layers in proton exchange membrane water electrolysis, Electrochim. Acta 354 (2020) 136641, https://doi.org/10.1016/j.electacta.2020.136641.
[12] M. Maier, K. Smith, J. Dodwell, G. Hinds, P.R. Shearing, D. Brett, Mass transport in PEM water electrolysers: a review, Int. J. Hydrogen Energy 47 (1) (2022) 30–56, https://doi.org/10.1016/j.ijhydene.2021.10.013.
[13] I. Dedigama, P. Angeli, K. Ayers, J.B. Robinson, P.R. Shearing, D. Tsaoulidis, et al., In situ diagnostic techniques for characterisation of polymer electrolyte membrane water electrolysers – flow visualisation and electrochemical impedance spectroscopy, Int. J. Hydrogen Energy 39 (9) (2014) 4468–4482.
[14] J. Parra-Restrepo, R. Bligny, J. Dillet, S. Didierjean, D. Stemmelen, C. Moyne, et al., Influence of the porous transport layer properties on the mass and charge transfer in a segmented PEM electrolyzer, Int. J. Hydrogen Energy 45 (15) (2020) 8094–8106.
[15] C. Immerz, B. Bensmann, P. Trinke, M. Suermann, R. Hanke-Rauschenbach, Local current density and electrochemical impedance measurements within 50 cm single-channel PEM electrolysis cell, J. Electrochem. Soc. 165 (16) (2018) F1292–F1299, https://doi.org/10.1149/2.0411816jes.
[16] D. Klotz, Negative capacitance or inductive loop? – a general assessment of a common low frequency impedance feature, Electrochem. Commun. 98 (2019) 58–62, https://doi.org/10.1016/j.elecom.2018.11.017.
[17] A. Schiefer, M. Heinzmann, A. Weber, Inductive low-frequency processes in PEMFC-impedance spectra, Fuel Cell. 20 (4) (2020) 499–506, https://doi.org/10.1002/fuce.201900212.
[18] C. Gerling, M. Hanauer, U. Berner, K.A. Friedrich, Experimental and numerical investigation of the low-frequency inductive features in differential PEMFCs: ionomer humidification and platinum oxide effects, J. Electrochem. Soc. 170 (1) (2023) 14504, https://doi.org/10.1149/1945-7111/acb3ff.
[19] S. Cruz-Manzo, P. Greenwood, Low frequency inductive loop in EIS measurements of an open-cathode polymer electrolyte fuel cell stack. Impedance of water vapour diffusion in the cathode catalyst layer, J. Electroanal. Chem. 900 (2021) 115733, https://doi.org/10.1016/j.jelechem.2021.115733.
[20] T. Ferriday, P.H. Middleton, Experimental analysis of materials in proton exchange membrane electrolysis cells, Int. J. Hydrogen Energy 44 (51) (2019) 27656–27663, https://doi.org/10.1016/j.ijhydene.2019.09.020.
[21] N. Hensle, D. Brinker, S. Metz, T. Smolinka, A. Weber, On the role of inductive loops at low frequencies in PEM electrolysis, Electrochem. Commun. 155 (2023) 107585, https://doi.org/10.1016/j.elecom.2023.107585.
[22] S de Angelis, T. Schuler, M.A. Charalambous, F. Marone, T.J. Schmidt, F.N. Büchi, Unraveling two-phase transport in porous transport layer materials for polymer electrolyte water electrolysis, J. Mater. Chem. A 9 (38) (2021) 22102–22113, https://doi.org/10.1039/D1TA03379D.
[23] A. Kalinnikov, S.A. Grigoriev, D.G. Bessarabov, K. Bouzek, Two-phase mass transfer in porous transport layers of the electrolysis cell based on a polymer electrolyte membrane: analysis of the limitations, Electrochim. Acta 387 (2021) 138541, https://doi.org/10.1016/j.electacta.2021.138541.
[24] J.K. Lee, C. Lee, K.F. Fahy, B. Zhao, J.M. LaManna, E. Baltic, et al., Critical current density as a performance indicator for gas-evolving electrochemical devices, Cell Reports Physical Science 1 (8) (2020) 100147, https://doi.org/10.1016/j.xcrp.2020.100147.
[25] G. Schmidt, M. Suermann, B. Bensmann, R. Hanke-Rauschenbach, I. Neuweiler, Modeling overpotentials related to mass transport through porous transport layers of PEM water electrolysis cells, J. Electrochem. Soc. 167 (11) (2020) 114511, https://doi.org/10.1149/1945-7111/aba5d4.
[26] C.C. Weber, T. Schuler, R de Bruycker, L. Gubler, F.N. Büchi, S de Angelis, On the role of porous transport layer thickness in polymer electrolyte water electrolysis, Journal of Power Sources Advances 15 (2022) 100095, https://doi.org/10.1016/j.powera.2022.100095.
[27] C.C. Weber, J.A. Wrubel, L. Gubler, G. Bender, S de Angelis, F.N. Büchi, How the porous transport layer interface affects catalyst utilization and performance in polymer electrolyte water electrolysis, ACS Appl. Mater. Interfaces 15 (29) (2023) 34750–34763, https://doi.org/10.1021/acsami.3c04151.
[28] T. Lickert, S. Fischer, J.L. Young, S. Klose, I. Franzetti, D. Hahn, et al., Advances in benchmarking and round robin testing for PEM water electrolysis: reference protocol and hardware, Appl. Energy 352 (2023) 121898, https://doi.org/10.1016/j.apenergy.2023.121898.
[29] T. Lickert, M.L. Kiermaier, K. Bromberger, J. Ghinaiya, S. Metz, A. Fallisch, et al., On the influence of the anodic porous transport layer on PEM electrolysis performance at high current densities, Int. J. Hydrogen Energy 45 (11) (2020) 6047–6058, https://doi.org/10.1016/j.ijhydene.2019.12.204.
[30] O. Sorsa, J. Nieminen, P. Kauranen, T. Kallio, Stable reference electrode in polymer electrolyte membrane electrolyser for three-electrode measurements, J. Electrochem. Soc. 166 (16) (2019) F1326–F1336, https://doi.org/10.1149/2.0461916jes.
[31] Z. Siroma, R. Kakitsubo, N. Fujiwara, T. Ioroi, S.-I. Yamazaki, K. Yasuda, Compact dynamic hydrogen electrode unit as a reference electrode for PEMFCs, J. Power Sources 156 (2) (2006) 284–287, https://doi.org/10.1016/j.jpowsour.2005.05.045.
[32] S. Adler, B. Henderson, M. Wilson, D. Taylor, R. Richards, Reference electrode placement and seals in electrochemical oxygen generators, Solid State Ionics 134 (1–2) (2000) 35–42, https://doi.org/10.1016/S0167-2738(00)00711-6.
[33] D. Gerteisen, Realising a reference electrode in a polymer electrolyte fuel cell by laser ablation, J. Appl. Electrochem. 37 (12) (2007) 1447–1454, https://doi.org/10.1007/s10800-007-9352-y.
[34] D. Gerteisen, Investigation of Dominant Loss Mechanisms in Low-Temperature Polymer Electrolyte Membrane Fuel Cells, Konstanz, Dissertation, 2009.
[35] S.B. Adler, Reference electrode placement in thin solid electrolytes, J. Electrochem. Soc. 149 (5) (2002) E166, https://doi.org/10.1149/1.1467368.
[36] S. Wang, J. Zhang, O. Gharbi, V. Vivier, M. Gao, M.E. Orazem, Electrochemical impedance spectroscopy, Nat Rev Methods Primers 1 (1) (2021), https://doi.org/10.1038/s43586-021-00039-w.
[37] M.E. Orazem, B. Tribollet, Electrochemical Impedance Spectroscopy, second ed., Wiley, Hoboken New Jersey, 2017.
[38] A. Lasia, Electrochemical Impedance Spectroscopy and its Applications, Springer New York, New York, NY, 2014.
[39] B.A. Boukamp, A linear kronig-kramers transform test for immittance data validation, J. Electrochem. Soc. 142 (1995), https://doi.org/10.1149/1.2044210.
[40] M. Schönleber, D. Klotz, E. Ivers-Tiffée, A method for improving the robustness of linear kramers-kronig validity tests, Electrochim. Acta 131 (2014) 20–27, https://doi.org/10.1016/j.electacta.2014.01.034.
[41] A. Leonide, V. Sonn, A. Weber, E. Ivers-Tiffée, Evaluation and modeling of the cell resistance in anode-supported solid oxide fuel cells, J. Electrochem. Soc. 155 (2008) B36–B41, https://doi.org/10.1149/1.2801372.
[42] H. Schichlein, A.C. Müller, M. Voigts, A. Krügel, E. Ivers-Tiffée, Deconvolution of electrochemical impedance spectra for the identification of electrode reaction mechanisms in solid oxide fuel cells, J. Appl. Electrochem. 32 (2002) 875–882, https://doi.org/10.1023/A:1020599525160.
[43] A.N. Tikhonov, A. Gončarskij, V.V. Stepanov, A.G. Jagola (Eds.), Numerical Methods for the Solution of Ill-Posed Problems, Springer, Dordrecht, 1995.
[44] E. Ivers-Tiffée, A. Weber, Evaluation of electrochemical impedance spectra by the distribution of relaxation times, J. Ceram. Soc. Japan 125 (4) (2017) 193–201, https://doi.org/10.2109/jcersj2.125.P4-1.
[45] M. Heinzmann, A. Weber, E. Ivers-Tiffée, Advanced impedance study of polymer electrolyte membrane single cells by means of distribution of relaxation times, J. Power Sources 402 (2018) 24–33.
[46] H. Göhr, C.-A. Schiller, Faraday-Impedanz als Verknüpfung von Impedanzelementen, Z. Phys. Chem. 148 (1) (1986) 105–124, https://doi.org/10.1524/zpch.1986.148.1.105.
[47] C.A. Schiller, F. Richter, E. Gülzow, N. Wagner, Relaxation impedance as a model for the deactivation mechanism of fuel cells due to carbon monoxide poisoning, Phys. Chem. Chem. Phys. 3 (11) (2001) 2113–2116, https://doi.org/10.1039/b007674k.
[48] D. Brinker, N. Hensle, J. Horstmann de la Viña, I. Franzetti, L.V. Bühre, U. A. Andaluri, et al., Research Data of the Publication *Inductive Loops in Impedance Spectra of PEM Water Electrolyzers*. KITopen Repository, 2024, https://doi.org/10.35097/KUsZkubcrDwyvyjm.
[49] Q. Meyer, C. Zhao, Air perturbation-induced low-frequency inductive electrochemical impedance arc in proton exchange membrane fuel cells, J. Power Sources 488 (2021) 229245.
[50] I. Pivac, F. Barbir, Inductive phenomena at low frequencies in impedance spectra of proton exchange membrane fuel cells – a review, J. Power Sources 326 (2016) 112–119, https://doi.org/10.1016/j.jpowsour.2016.06.119.
[51] T. Hrbek, P. Kúš, M.G. Rodríguez, V. Matolín, I. Matolínová, Operando X-ray photoelectron spectroscopy cell for water electrolysis: a complete picture of iridium electronic structure during oxygen evolution reaction, Int. J. Hydrogen Energy 57 (2024) 187–197, https://doi.org/10.1016/j.ijhydene.2023.12.216.